DEPARTAMENTO DE CIÊNCIAS DOS MATERIAIS

Inês Gonçalves Dias
Licenciada em Engenharia de Micro e Nanotecnologias

MAGNETIC DENDRIMERS FOR BONE METASTASES THERANOSTICS AND BONE REGENERATION

MESTRADO INTEGRADO EM ENGENHARIA DE MICRO E NANOTECNOLOGIAS
Universidade NOVA de Lisboa
Março, 2023

DEPARTAMENTO DE CIÊNCIAS DOS MATERIAIS

MAGNETIC DENDRIMERS FOR BONE METASTASES THERANOSTICS AND BONE REGENERATION

INÊS GONÇALVES DIAS

Licenciada em Engenharia de Micro e Nanotecnologias

Orientador: Doutor Vasco D. B. Bonifácio
Professor Auxiliar do Departamento de Bioengenharia do Instituto Superior Técnico da Universidade de Lisboa

Coorientadores: Doutor João Paulo M. R. Borges,
Professor Associado com Agregação do Departamento de Ciência dos Materiais da FCT NOVA

Júri:

Presidente: Doutora Maria Helena Figueiredo Godinho,
Professora Associada com Agregação do Departamento de Ciência dos Materiais da FCT NOVA

Arguentes: Doutora Rita Figueiredo Pires,
Investigadora Júnior do Centro de Física e Engenharia de Materiais Avançados do Instituto Superior Técnico da Universidade de Lisboa

Orientador: Doutor Vasco Daniel Bigas Bonifácio,
Professor Auxiliar do Departamento de Bioengenharia do Instituto Superior Técnico da Universidade de Lisboa

MESTRADO INTEGRADO EM MICRO E NANOTECNOLOGIAS

Universidade NOVA de Lisboa

Março, 2023

Magnetic Dendrimers for Bone Metastases Theranostics and Bone Regeneration

Para o meu avô Eduardo,

AGRADECIMENTOS

Em primeiro lugar, gostaria de agradecer aos meus orientadores, Prof. Dr. Vasco Bonifácio e Prof. Dr. João Paulo Borges pela disponibilidade e orientação durante todo o meu percurso. Gostaria também de fazer um agradecimento especial à Prof. Dra. Paula Soares, que me orientou em tudo o que se relacionava com nanopartículas e que se disponibilizou para ajudar quando necessário; e à Dra. Tânia Vieira, que me deu todo o apoio necessário para fazer os ensaios celulares, me ajudou a arranjar soluções para os problemas que encontrávamos pelo caminho e, sobretudo manteve a paciência, após inúmeras contaminações que nos obrigaram a estender os testes.

Gostaria também de agradecer à Prof. Dra. Paula Soares pelas medidas de hipertermia magnética, à Prof. Dra. Marta Corvo pela caracterização feita por RMN e ao MicroLab do Instituto Técnico de Lisboa por me possibilitar obter análises por TEM.

Gostaria de agradecer à Adriana Gonçalves por ter estado sempre presente ao longo deste percurso, através de sessões de brainstorming, ajuda em experiências e todo o apoio emocional e companhia, sem o qual, terminar esta tese teria sido muito mais difícil. Não me posso esquecer de agradecer também à Catarina Chaparro, que embora sempre ocupada e a trabalhar em vários sítios ao mesmo tempo, tirou bocadinhos do seu dia para me responder a inúmeras perguntas e me aconselhar, consoante a sua experiência, quais os procedimentos a seguir. E ao Francisco, não sei sequer como te agradecer por teres estado comigo desde o primeiro ano de faculdade até ao último, por me teres ajudado com trabalhos de grupos a testes, por teres ouvido todas as minhas frustrações e teres partilhado as tuas, fizeste o meu percurso de faculdade melhor. Obrigada por tudo.

E, por fim, tenho de agradecer à minha família e aos meus amigos, que tiveram sempre presentes para mim. Não poderia ter chegado tão longe sem o vosso apoio.

“Learning is not compulsory, but neither is survival.”

(William Deming)

ABSTRACT

Some of the most incident cancers metastasize to the bone which leads to a long clinical course and a short prognosis. In this work, it was developed a hybrid system composed of superparamagnetic iron oxide nanoparticles (SPIONs) functionalized with polyurea oxide (PURO) dendrimers or branched poly(ethylene imine) oxide (BOXI-PEI). SPIONs are used for magnetic fluid hyperthermia and have been clinically approved as contrast agents in magnetic resonance imaging, while PURO dendrimers have been proven to trigger osteogenic differentiation of human mesenchymal stem cells (hMSCs). The functionalization of SPIONs with PURO biodendrimers allows the construction of a platform with potential for therapy and bone regeneration while being able to monitor the therapeutic response.

After the synthesis of the SPIONs, and the coating polymers, the method for surface coating of the nanoparticles was optimized. The obtained devices obtained were characterized in terms of structural, morphological, and chemical by standard methods like dynamic light scattering (DLS), zeta potential, and transmission electron microscopy (TEM), and stable nanoparticles with a diameter of around 10 nm and neutral charge were obtained. To evaluate the device's theranostic ability, the heating capacity and their relaxation time were evaluated by magnetic hyperthermia and nuclear magnetic resonance, respectively. Furthermore, cytotoxicity assays were performed to access the biocompatibility of the system.

Keywords: Superparamagnetic iron oxide nanoparticles; polyurea oxide; branched poly(ethylene imine); cancer theranostic; osteogenic differentiation; bone regeneration.

RESUMO

Alguns dos cancros com maior incidência metastizam no osso, o que origina longos percursos clínicos e baixos prognósticos. Neste trabalho, foi desenvolvido um sistema híbrido, composto com nanopartículas superparamagnéticas de óxido de ferro (SPIONs) funcionalizadas com dendrímeros de óxido de poliureia (PURO) ou polímeros ramificados de óxido de poli(etileno imina) (BOXI-PEI). Os SPIONs são usados para hipertermia fluída magnética e foram aprovadas clinicamente como agentes de contraste em ressonâncias magnéticas, enquanto os dendrímeros PURO fazem a diferenciação osteogénica de células humanas do mesênquima. A funcionalização dos SPIONs com estes polímeros permite o desenvolvimento de uma plataforma com potencial terapêutico e de regeneração óssea, e também monitorizar a resposta terapêutica.

Após a síntese dos SPIONs e dos polímeros de revestimento, o método para revestir a superfície das nanopartículas foi otimizada e os dispositivos obtidos foram caracterizados em termos de estrutura, morfologia e química por métodos *standard* tais como espalhamento dinâmico de luz (DLS), potencial zeta e microscopia eletrónica de transmissão (TEM), onde foi possível obter nanopartículas estáveis com um diâmetro cerca de 10 nm e com carga neutra. Para avaliar a capacidade teranóstica do dispositivo, a sua capacidade de aquecimento por hipertermia magnética e o seu tempo de relaxação por ressonância magnética nuclear foram quantificadas. Além disso, foram feitos ensaios de citotoxicidade para avaliar a biocompatibilidade do sistema.

Palavras-Chave: Nanopartículas superparamagneticas de óxido de ferro; óxido de dendrímero de poliureia; óxido de poli(etileno imina) ramificada; agentes teranósticos para cancro; diferenciação osteogénica; regeneração óssea.

Contents

LIST OF FIGURES

LIST OF TABLES

LIST OF ABBREVIATIONS

ALP	Alkaline Phosphatase
APTES	(3-aminopropyl)triethoxysilane
ATP	Adenosine Triphosphate
b-PEI	Branched Poly(ethylene imine)
BOXI-PEI	Branched Oxide Poly(ethylene imine)
CA	Citric Acid
DLS	Dynamic Light Scattering
DMSA	Simercaptosuccinic acid
H_2O_2	Hydrogen Peroxide
HA	Hydroxyapatite
hMSCs	Human Mesenchymal Stem Cells
l-PEI	Linear Poly(ethylene imine)
MFH	Magnetic Fluid Hyperthermia
MRI	Magnetic Resonance Imaging
NMR	Nuclear Magnetic Resonance
NO	Nitric Oxide
NPs	Nanoparticles
PAMAM	Poly(amidoamine)
PURE	Polyurea
$PURE_{G4}$	Polyurea Generation 4
PURO	Polyurea Oxide
$PURO_{G4}$	Polyurea Oxide Generation 4
SAR	Specific Absorption Rate
SPIONs	Superparamagnetic Iron Oxide Nanoparticles
SQUID	Superconducting Quantum Interference Device
TEM	Transmission Electron Microscopy

MOTIVATION

Lung, breast, and prostate cancers are some of the most common cancers in the world, according to the World Health Organization, that metastasize to the bone [1]. Bone metastases reflect a high incidence (65-75% in breast cancer, 65-75% in prostate cancer, and 30-40% in lung cancer), a long clinical course, and a short prognosis, characterized by severe pain, impaired mobility, spinal cord compressions, and pathologic fractures [2].

Bone is continuously remodeled through a balanced sequence of bone resorption by osteoclasts and subsequent bone formation by osteoblasts, which results in the replacement of old bone with new, allowing the structural integrity of the skeleton [3,4]. Bone metastasis affects the balance of osteoclast and osteoblast numbers and activity, which results in the disturbance of bone remodeling [2,5]. It can be classified, according to the primary mechanism of interference with the bone remodeling, as osteolytic, osteoblastic, or mixed [3]. Osteolytic metastasis is characterized by the destruction of normal bone, mainly present in breast cancer [3]. The lesions are not a direct effect of the tumor cells but, of the osteoclast-activating factors released in the bone microenvironment, which leads to increased bone fragility, susceptibility to fracture, and pathological fractures, often occurring in load-bearing bones like the femur or the pelvis [3,6]. Osteoblastic metastasis is characterized by the deposition of new bone, while mixed metastasis has both osteolytic and osteoblastic lesions [3].

Even though there are treatments that can help with the symptoms or slow the growth of bone metastases, they rarely can be cured [3]. Among several other treatments, the most relevant are the use of bisphosphonates, radiotherapy, and surgery. Bisphosphonates bind to the mineralized bone surface and inhibit osteoclastic bone resorption. They have been shown to reduce pain and the risk of skeletal-related events, while having antitumoral activity [2,3,7]. Radiotherapy has been an established treatment for the management of bone metastases for many decades, which can achieve a significant pain response and reduction in complication rates [7]. Surgery can only be performed in specific cases, but it is essential to stabilize the bone, avoid pathological fractures, and deal with spinal compressions [3]. Moreover, a combination of these treatments can be used to achieve a better, more personalized outcome.

This dissertation has the objective of developing a hybrid therapeutic formulation comprising of superparamagnetic iron oxide nanoparticles (SPIONs) functionalized with polyurea oxide (PURO) biodendrimers. This system will take advantage of the theranostic properties of SPIONs and the bone regeneration properties of PURO, adding a new possible diagnosis and treatment for bone metastases to be used independently or in combination with other treatments.

1. INTRODUCTION

1.1. MAGNETIC NANOPARTICLES

Nanoparticles (NPs) are, by definition, nanostructures with at least one dimension below 100 nm [8]. These types of structures have been gaining increasing interest in the last decades, since, at the nanoscale, materials have shown to have different properties from those of bulk materials. They have been extensively studied for biomedical applications, including for novel applications in cancer treatment [8].

Magnetic nanoparticles, nanostructures that can be manipulated with an external magnetic field, can be composed of pure metals, metal alloys, or metal oxides. The usual choice for biomedical applications are metal oxide NPs, especially iron oxide, due to their biocompatibility, superparamagnetic properties, and chemical stability under physiological conditions [8,9].

Materials can be divided into diamagnetic, ferromagnetic, and paramagnetic based on their response to a magnetic field. Diamagnetism is a weak, non-permanent form of magnetism, characterized by a small induced magnetic moment and in the opposite direction of the applied magnetic field. It can only be observed if no other forms of magnetism are present [10]. Ferromagnetism occurs in particles whose unpaired electron spins align themselves spontaneously, in domains, leading to magnetization even in the absence of an applied magnetic field [8]. When the size of the ferromagnetic particles decreases below a critical size, it will present a single magnetic domain, leading to paramagnetic properties. When the size of the single-domain particles further decreases, the coercivity goes from its maximum value to zero and the particles become superparamagnetic (Figure 1.1) [8,9].

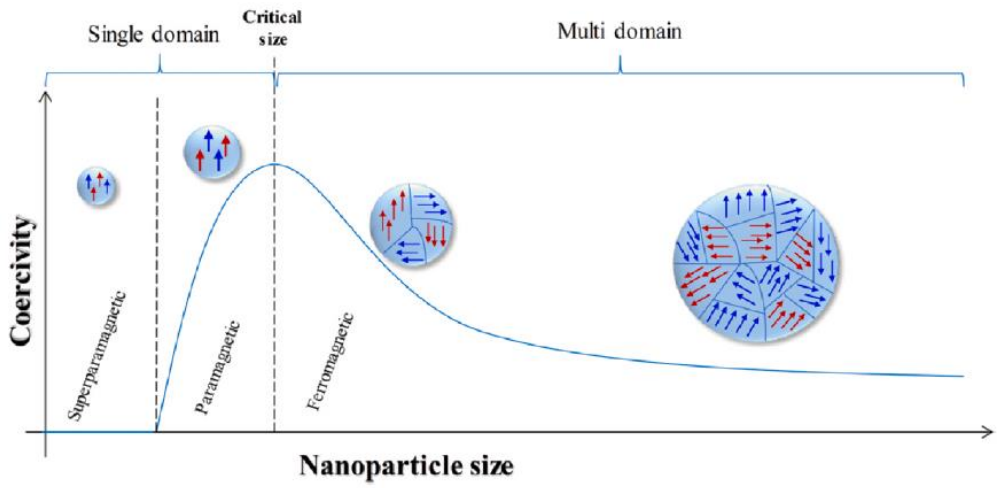

Figure 1.1 - Correlation between particle size, coercive field, and magnetic domain structures [8].

1.1.1. Superparamagnetic Iron oxide nanoparticles

Superparamagnetic NPs can rapidly change their magnetic state with the application of an external alternating magnetic field. Since their coercivity is zero, as the field is removed no residual magnetization is left, avoiding an "active behavior" (Figure 1.2) [8,9].

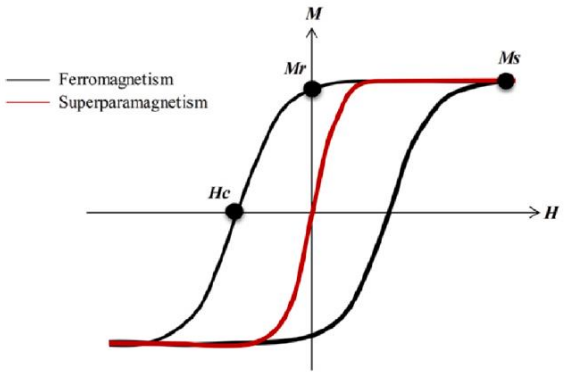

Figure 1.2 – Schematic representation of hysteresis loop (magnetization (M) vs applied field (H)) for ferromagnetic and superparamagnetic materials (Ms – Saturation magnetization; Hc - coercive field; Mr - remanent magnetization) [8].

An important characteristic of NPs, particularly in biomedical applications, is their colloidal stability. When in aqueous solutions, NPs tend to aggregate leading to larger particles with higher sedimentation rates. To avoid such aggregation, a coating can be added during or after the particle synthesis, which will act as a stabilizer, maintaining their initial properties. The coating should be both biocompatible and biodegradable, without negatively affecting the magnetic properties [8,9]. Additionally, the coating can add specific functionalities like specific targeting for drug delivery or fluorescence imaging.

In the biomedical field, SPIONs can be used in cancer theranostic applications, that is, applications that combine both diagnosis and therapy leading to a possible earlier diagnosis and more personalized treatment [11]. Some examples of applications are:

- Contrast Agents for Magnetic Resonance Imaging (MRI): MRI is an established diagnosis method since it's a non-invasive technique that allows the observation of physiological phenomena with soft tissue differentiation. SPIONs have already been approved and used in clinical settings as negative contrast agents in T2-weighted images [12].

- Magnetic Fluid Hyperthermia (MFH): In MFH, superparamagnetic NPs are dispersed in the cancerous tissue, when an external alternating magnetic field is applied with enough strength and frequency, the NPs induce heat generation. If the temperature is maintained above the threshold of 42ºC, the tumor will be destroyed, since tumor cells are known to be more sensitive to temperature increases in comparison with healthy ones. When functionalizing the NPs, it is important to note that the coating can shield off the particles significantly affecting their application in MFH [8,9].

- Drug Delivery: Drug delivery systems transport a specific drug to the targeted site, having the advantage of using a lower dose and reducing undesired side effects. Since superparamagnetic NPs can be functionalized with reversibly bound drugs, it's possible to use external magnetic fields to release them to a specific location. Moreover, it's also possible to functionalize the particles with fluorescent probes, for the monitorization of the path followed [8,9].

1.2. Dendrimers

Synthetic polymers are divided into 4 different architectural categories: linear, cross-linked, branched, and dendritic. Dendrimers or dendritic structures are characterized by having a well-defined and highly branched 3D architecture, composed of a central core, branched units, and a high number of terminal groups (Figure 1.3) [13]. The branching units are organized in layers called generations, which are composed of repeating monomer units; as the number of generations increases, the central core gets more shield from the core.

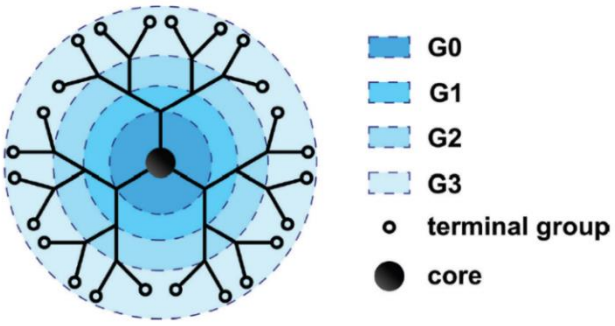

Figure 1.3 – Schematic representation of a dendrimer [14].

The dendrimers synthesis can be divided into convergent and divergent. While the convergent synthesis starts from the branches, the divergent method starts with the core. In both methods, the dendrimer grows generation by generation from the reaction with monomer units, their building blocks, leading to a precise and controlled architecture with predictable molecular weights [15]. Due to their unique properties, dendrimers have been applied in the most diverse fields, including in the biomedical area. Some examples of applications are drug delivery; gene therapy; imaging; cancer therapy and tissue regeneration.

1.2.1. Polyurea Oxide Dendrimers and Branched Oxide Poly(ethylene)Imine

Polyurea (PURE) dendrimers are described as being biocompatible, biodegradable, and non-cytotoxic [16,17]. These are composed of tertiary amines and urea groups, with primary amines as their terminal groups. Since amines are prone to chemical oxidation, it is possible to oxidize them to get the corresponding PURO dendrimers. Using hydrogen peroxide (H_2O_2) as an oxidant, there will be the formation of *N*-oxides from the tertiary amines and hydroxylamines from the primary amines (Figure 1.4a) [16].

Pires *et al.* [16] demonstrated that PURO dendrimers trigger osteogenic differentiation of human mesenchymal stem cells (hMSCs). In this work was postulated that the PURO hydroxylamine-terminated surface, resulting from the oxidation of surface primary amines of the PURE dendrimers precursor, leads to *in situ* nitric oxide (NO) release by the action of catalase (Figure 1.4b) [16]. Recently this mechanism was proved by studying NO release by fluorescence spectroscopy (unpublished data). It has been already demonstrated that an increase in alkaline phosphatase (ALP) activity, an established biomarker for osteoblast activity, is connected to the increase in NO [16].

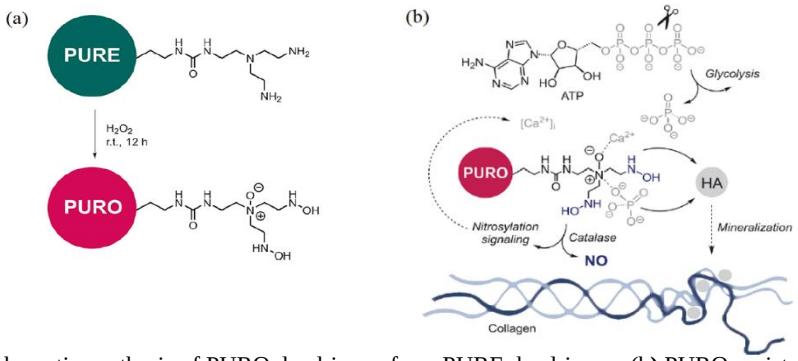

Figure 1.4 - (a) Schematic synthesis of PURO dendrimers from PURE dendrimers, (b**)** PURO-assisted osteogenic differentiation of hMSCs [16].

Branched poly(ethylene imine) (b-PEI) is a commercially available branched polymer with the same terminal groups as PURE dendrimers, which can be oxidized, and form branched oxide poly(ethylene imine) (BOXI-PEI), a PURO counterpart. BOXI-PEI, displaying similar NO release potential, could be a simple and cost-effective alternative to PURO.

1.3. Dendrimers and Nanoparticles Complexes

The combination of nanoparticles and dendrimers is possible by different approaches: i) by the encapsulation of a single nanoparticle within a single dendrimer, where this last can be used as a template to tune the size of the nanoparticle; ii) by the formation of NPs between dendrimers, which will lead to larger NPs than the first method; iii) by the coating of NPs with dendrons instead of dendrimers; and iv) by directing the NPs placement with dendrimers towards 2D and 3D structures [18].

The combination of the unique properties of both dendrimers and magnetic nanoparticles, for cancer theranostics, has been already reported [19,20]. Haribabu *et al.* developed manganese-doped iron nanoparticles entrapped in poly(amidoamine) (PAMAM) dendrimers with both T1 and T2 contrasting ability in MRI [21]. Chang *et al.* presented a pH-responsive drug carrier, where doxorubicin, a common anticancer drug, is entrapped in PAMAM dendrimers modified with poly(ethylene glycol) and attached to iron oxide nanoparticles, with the objective of having a targeted delivery, avoiding the cardiac toxicity of doxorubicin [22]. In its work, stable complexes with pH-controlled activation were obtained with the possibility, due to the presence of the iron oxide nanoparticles, of being used as an MRI probe to follow the course of the delivering drug [22]. There have been also recent advancements in the use of nanoplatforms for the treatment of osteosarcoma, the most common primary bone tumor in children, including complexes that include dendrimers and nanoparticles [23]. In the work of Niew *et al.*, it was developed a melatonin and doxorubicin drug delivery system by joining amine/functionalized β-cyclodextrin grafted graphene oxide with iron oxide nanoparticles loaded with an anticancer drug. The result was a stable high-loading nanocarrier with low toxicity and favorable biocompatibility [24].

In this project, SPIONs and PURO dendrimers (or, alternatively, BOXI-PEI) were combined to create a theranostic platform for bone metastases therapy through magnetic hyperthermia and, simultaneously, bone regeneration. Furthermore, their structural, morphological, and chemical properties and their cytotoxicity will be studied as their capacity to act as an MRI contrast agent.

2. MATERIALS AND METHODS

2.1. PURO DENDRIMERS AND BOXI-PEI POLYMERS SYNTHESIS

The synthesis of PURO dendrimers is achieved by the oxidation of the corresponding PURE dendrimers following the protocol described by Pires *et al.* [16]. Briefly, 0.50 mL of 35% w/w hydrogen peroxide (H_2O_2) was added dropwise to 50 mg of $PURE_{G4}$. The solution was diluted with water and dialyzed for at least 24 hours. After, the solution is evaporated to give the pure $PURO_{G4}$ dendrimer as a light-yellow oil. ^{1}H-NMR (D_2O, 400 MHz) δ (ppm): 3.74-3.44 (CH_2, m), 1.96 and 1.90 (NH). The nuclear magnetic resonance (NMR) spectra before ($PURE_{G4}$) and after oxidation ($PURO_{G4}$) is shown in Appendix A.1.1.

The synthesis of BOXI-PEI was achieved by the oxidation of b-PEI ($H(NHCH_2CH_2)_nNH_2$, *Sigma-Aldrich*), the method of oxidation is the same as the one described for the $PURE_{G4}$ dendrimers. A similar protocol to the one described by Englert *et al.* [25], where a mixture of methanol and water was used as the solvent of linear poly(ethylene imine) (l-PEI) for its oxidation with H_2O_2, was followed where methanol was used as solvent before the addition of the hydrogen peroxide. ^{1}H-NMR (D_2O, 400 MHz) δ (ppm): 3.96-3.53 (CH_2, m). The NMR spectra before (b-PEI) and after oxidation (BOXI-PEI) is shown in Appendix A.1.2.

2.2. SPIONS SYNTHESIS

SPIONs are synthesized by chemical co-precipitation following the method described by Soares *et al.* [26], using 2.5 mmol of iron (II) chloride tetrahydrate ($FeCl_2.4H_2O$, 98%, *Alfa Aesar*) and 5 mmol iron (III) chloride hexahydrate ($FeCl_3.6H_2O$, 97%, *Sigma-Aldrich*). The nanoparticles were washed at least three times and since, in this case, no dialysis was performed, the pH of the solution was measured to assure that no ammonia was left. If the pH was still not neutral, the solution was once again washed until it was.

The iron content in the SPIONs solution was determined using the 1,10-phenantroline colorimetric method, in order to quantify the amount of stabilizer to add to the NPs [26,27]. The SPIONs solution was stored at 9ºC and whenever it was necessary to use the solution, this one was sonicated with a tip sonicator to get a uniform solution.

2.3. SPIONs Surface Coating

For the coating of the SPIONs when using citric acid (CA), the method demonstrated by Dheyab *et al.* [27] was followed with slight modifications. Briefly, 0.5 g of CA ($HOC(COOH)CH_2COOH)_2$, *Sigma-Aldrich*) was added, while the solution of SPIONs was mechanically stirred at 650 rpm for 30 minutes at room temperature. When the BOXI-PEI was added, in a ratio 1:2 (SPIONs:BOXI-PEI), mechanical agitation was maintained using an orbital shaker for 24 hours at 210 rpm. The second method tried, the b-PEI was added to CA with the intent of neutralizing it, before its addition to the SPIONs. The solution was then mechanically stirred for 30 minutes at 210 rpm. After each stabilization, the nanoparticles were collected with a magnet confirming their magnetic properties, while removing any surfactant that didn't react, to further characterize the SPIONs.

For the stabilization of SPIONs with only PURO or BOXI-PEI, the first method tried was a simple addition, the BOXI-PEI was added to the solution of SPIONs, with a ratio of 1:1 and the final solution was mechanically stirred using an orbital shaker at 210 rpm for 24 hours (Method 1). The second method tried, the BOXI-PEI was added right after the SPIONs synthesis without stopping the vigorous mechanical stirring used during the synthesis, for 30 minutes at room temperature (Method 2). The last method tried, PURO or BOXI-PEI was added to the SPIONs solution and maintained in an ultrasonic bath for 1 hour and 30 min (Method 3). The stabilized nanoparticles were collected with a magnet, confirming their magnetic properties, and removing any polymer that didn't react, to be further characterized.

2.4 Complexes Characterization

The particle sizes and zeta potential were obtained through Dynamic Light Scattering (DLS), using *SZ-100 nanopartica series* (*Horiba, Lda*).The samples were diluted at 1:150 using filtered water to decrease possible contaminants. For each analysis, 3 measurements were made during 30 seconds with 5 seconds of delay in between. For the Transmission Electron Microscopy (TEM), each solution of nanoparticles was diluted and placed in a Kevlar 25 mesh grid. The TEM images were obtained in a Hitachi H-8100 II with thermionic emission LaB6 and the size distribution was calculated using *ImageJ*™ software. The magnetic hyperthermia measurements were made using D5 of Nb Nanoscale Biomagnetics with a field intensity of 300 Gauss and a frequency of 388.4 kHz. The measurements were made after 30-40 seconds without the application of a magnetic field for the stabilization of the temperature, followed by 10 min of magnetic applied field. The NMR measurements were made in a Bruker Avance III NMR spectrometer in a 7 T magnetic field at 25 ºC. Two types of cytotoxicity assays were tried, the first was the resazurin assay and the protocol described by Vieira *et al.* [28] was followed. It's important to note, that to the culture medium used, upon adding the nanoparticles to the cells, 2 % of gentamincin reagent solution (*ThermoFisher*, 10 mg/mL) was added, to prevent the contamination of cell cultures by bacteria. The second was the live and dead assay, where a solution of calcein at 0.2 µL/mL and etidium at 0.8 µL/mL in serum free medium with 25 mM (4-(2-hydroxyethyl)-1-piperazineethanesulfonic acid. The culture medium was replaced with the prepared fresh solution. The samples are incubated for 30 minutes and, after it is washed with a complete culture medium with fetal bovine serum, and the samples were observed using Nikon Inverted microscope with 10x magnification.

3. Results and Discussion

3.1. Surface Coating Optimization

In this work, iron oxide nanoparticles were synthesized by a co-precipitation protocol. When suspended in water, the nanoparticles form an unstable colloidal suspension due to their positive charge. This instability leads to aggregation of the particles, increasing their size, which leads to higher sedimentation rates and different magnetic properties. One of the most effective ways to neutralize the nanoparticles and increase their colloidal stability is the addition of a coating. The dendrimers ($PURO_{G4}$) and the branched polymer (BOXI-PEI) used in this work have in their backbone *N*-oxide, which have been proven to be effective Fe^{2+}/Fe^{3+} chelators (a chemical compound that binds to metal ions), making them, in theory, a good coating for the nanoparticles in question [29]. One alternative option was the use of citric acid. Since CA was already extensively studied as a coating for iron oxide nanoparticles and is proven to lead to small stable superparamagnetic nanoparticles, these complexes of SPIONs plus CA could then be further functionalized with the dendrimers or branched polymers instead of these molecules having to completely surround the SPIONs, thus being necessary less quantity of polymer to have stable SPIONs with osteogenic differentiation properties [27].

3.1.1 Citric Acid and PURO or BOXI-PEI

Citric acid is easy to handle, toxicologically safe, highly water soluble and capable of acting as a strong chelator [30]. Moreover, citric acid when dissolved in water has negative charges and since PURO has both negative and positive charges, electrostatic binding could be possible.

Throughout this work, a DLS particle size distribution analysis was made with the objective of evaluating how appropriate the coating method of the SPIONs would be for our application. This was just a preliminary study and, further along, the work, after the coating method was optimized, a more complete characterization of the device was made. This is important to take note of as a DLS analysis allows us to obtain the hydrodynamic diameter of the NPs, which refers to the particle size of smooth, spherical particles which diffuse at the same speed as the particles of the sample, that is we are measuring the whole device, including the coating instead of having the diameter of only the iron oxide nanoparticle [31]. With that in mind, the objective is to have a colloidal solution with particles with a size range of approximately 10-100 nm, which is the ideal size range for the biodistribution of the particles; and with a polydispersity index as low as possible [8].

Table 3.1 – Dynamic light scattering characterization of SPIONs stabilized with CA, and with CA and BOXI-PEI.

	Polydispersity Index	Particle Diameter (nm)
SPIONs + CA	0.160	81.70
	0.180	86.90
	0.160	80.84
SPIONs + CA+ BOXI-PEI	3.66	$42.23x10^3$
	3.65	
	3.53	$40.85x10^3$

As seen in Table 3.1, when the BOXI-PEI was added, both the polydispersity index and the particle diameter showed a significant increase, leading us to believe that the particles, previously stable by the citric acid were destabilized, leading to further aggregation. It is thought that, since the BOXI-PEI has a high pH in comparison with the citric acid, when the polymer was added, the citric acid was rapidly converted into citrate, destabilizing the coating of the SPIONs. A table showing the comparison of the pH values of the different compounds used is available in Appendix Table A.2.1.

In an attempt to avoid the observed destabilization, CA was first neutralized with b-PEI (precursor of BOXI-PEI) before its addition to the SPIONs solution. For that and to maintain the acidity of the solution, 45 extra moles of CA per 0.33 mol of BOXI-PEI (or per each mol of $PURO_{G4}$) would be needed. We know that the molecular weight of b-PEI is 25 000 g/mol and of citric acid is 192.12 g/mol. Thus, for 0.50 g of citric acid, 0.48 g of b-PEI would be needed. This method showed some improvements with a slightly smaller polydispersity index and particle diameters, yet the values are still far from the ideal ranges.

Table 3.2- Dynamic light scattering characterization of SPIONs stabilized with CA and BOXI-PEI when citric acid was neutralized before being added to the solution.

	Polydispersity Index	Particle Diameter (nm)
SPIONs + CA+ BOXI-PEI	0.980	$10.98x10^3$
	1.64	$15.55x10^3$
	1.76	$19.16x10^3$

For the preliminary studies with the purpose of reaching an appropriate coating method, only the branched polymer, BOXI-PEI, was studied.

3.1.2 PURO OR BOXI-PEI

For the coating of the nanoparticles using dendrimers or, in alternative the branched polymers, three different methods were tried. For these preliminary studies, the ratio used of SPIONs:BOXI-PEI was of 1:1.25 with a SPIONs concentration of 14 mg/mL.

Comparing the three tried methods, it was possible to conclude that the third method, where the BOXI-PEI is added to the SPIONs , and the solution is maintained in an ultrasonic bath for 1 hour and 30 minutes would be the best method to follow. The ultrasonic bath allows, through high frequency and high

intensity sounds, the separation of the particles and avoids their aggregation, allowing the BOXI-PEI to surround the nanoparticles and stabilized them at a small size.

Table 3.3 – Dynamic light scattering characterization of SPIONs stabilized with BOXI-PEI with three different methods.

		Polydispersity Index	Particle Diameter (nm)
SPIONs + BOXI-PEI	Method 1	1.39	$14.28x10^3$
		1.61	$15.09x10^3$
		2.20	$19.55x10^3$
	Method 2	1.07	$29.85x10^3$
		2.08	$21.01x10^3$
		2.10	$21.98x10^3$
	Method 3	0.203	192.9
		0.162	185.5
		0.189	197.1

3.2. RATIO OPTIMIZATION

Table 3. Error! No text of specified style in document.**4 –** Dynamic light scattering characterization of SPIONs stabilized with different ratios of $PURO_{G4}$ and BOXI-PEI through Method 3. Mean ± Standard Deviation for every determination is shown.

	Ratio	Polydispersity Index	Particle Diameter (nm)
SPIONs + $PURO_{G4}$	1:2.5	0.980 ± 0.11	$16.79x10^2$ ± 20.32
	1:1.5	0.640 ± 0.060	504.3 ± 16.68
	1:1	0.330 ± 0.21	415.3 ± 18.88
	1:0.5	1.21 ± 0.18	$23.72x10^3$ ± 721.1
SPIONS + BOXI-PEI	1:1	0.150 ± 0.020	129.8 ± 0.9900
	1:0.5	0.140 ± 0.010	144.5 ± 7.350
	1:0.3	0.120 ± 0.070	139.1 ± 5.970
	1:0.1	0.140 ± 0.010	132.1 ± 2.040
	1:0.05	0.260 ± 0.030	140.3 ± 6.110

After finding the best method for SPIONs coating, the quantities of dendrimers or branched polymers were optimized in relation to the quantity of SPIONs. The same concentration of 3.12 mg/mL of SPIONs was used in every one of the determinations.

When comparing the DLS results of the different ratios, it was easy to choose the optimized ratio of the system SPIONs+$PURO_{G4}$ since there was such stark contrast between the results. Considering the smaller polydispersity index and particle diameter, the chosen ration of SPIONs:$PURO_{G4}$ was 1:1. In the case of the system SPIONs+BOXI-PEI all the ratios considered seem to result in low polydispersity indexes and diameters apt for our application. Therefore, a preliminary study of the colloidal stability of the different

ratios was made, in order to choose the best, more stable option to further characterize. For this preliminary study, all the samples were maintained at 9ºC for 30 days.

Table 3.5 – Dynamic Light Scattering characterization of SPIONs stabilized with BOXI-PEI after 30 days**.** Mean ± Standard Deviation for every determination is shown.

	Ratio	Polydispersity Index	Particle Diameter (nm)
SPIONS+BOXI-PEI	1:1	0.930 ± 1.1	$32.53x10^2$ ± 766.2
	1:0.5	0.190 ± 0.060	$31.39x10^2$ ± 251.4
	1: 0.3	0.120 ± 0.060	$43.50x10^2$ ± 276.4
	1:0.1	0.230 ± 0.010	$41.12x10^2$ ± 661.8
	1:0.05	0.760 ± 0.65	$50.93x10^2$ ± 1444

As it is possible to see on Table 3.5, after 30 days there was considerable particle aggregation and although we can't see a dramatic difference between results, the ratio chosen for the coating of BOXI-PEI for further characterization was 1:0.5, which ultimately showed the lowest polydispersity and particle diameter in this analysis.

For higher quantities of BOXI-PEI, for ratios of 1:1.25 and above, the solution appears to have a different behavior. Furthermore, a similar behavior was observed when to maintaining the optimal ratio of 1:0.5, we use high concentrations of nanoparticles (5 mg/mL and higher). In both these cases, no phase separation is observed when a magnetic field is applied, leading to difficulty in collecting the nanoparticles and separating them from the solvent and remaining polymer. Instead, the solvent, in this case, water moves together with the nanoparticles in the direction of the magnetic field, as seen in Figure 3.1, behaving similarly to a ferrofluid [32]. Ferrofluids are colloidal liquids that possess strong magnetic features whose physical properties can be controlled by the application of a magnetic field. They are composed of a ferromagnetic compound in a nanometer range, a surfactant or dispersant which coats the particles avoiding their aggregation, and a carrier liquid [32]. Ferrofluids also present a Rosensweig instability pattern of peaks and valleys observed by naked eye, which weren't observed in the solution seen in Figure 3.1. Through a DLS analysis with a dilution of 1:150, it was obtained a polydispersity index of 1.58 ± 0.57, a hydrodynamic diameter of $23.92x10^3 \pm 20.49x10^2$ nm, and zeta potential of -12.9 mV, which aren't close to the characteristic values of ferrofluid materials, nor the normal values obtained with the solution with the optimized ratio of SPIONs and BOXI-PEI [32]. It would be interesting to further characterize this solution through TEM and superconducting quantum interference device (SQUID) magnetometry.

a)  **b)** 

Figure 3.1 – a) SPIONs coated with $PURO_{G4}$, with the action of a magnet it is possible to see the separation of SPIONs and supernatant; b) SPIONs coated with BOXI-PEI with high concentration, no separation exists, instead the whole solution is affected by the magnet.

3.3. Complexes Characterization

3.3.1. DLS

Table 3.6 shows a summary of the results obtained through DLS analysis with the optimized synthesis method and ratios, where it is possible to see how the coatings used, reduce the hydrodynamic diameter and polydispersity indexes.

Table 3.1 – Dynamic light scattering characterization of uncoated SPIONs and of the optimized ratios of coating with $PURO_{G4}$ and BOXI-PEI. Mean ± Standard Deviation for every determination is shown.

	Ratio	Polydispersity Index	Particle Diameter (nm)
Uncoated SPIONs	-	0.140 ± 0.020	$73.30x10^2$ ± 1720
SPIONs + $PURO_{G4}$	1:1	0.330 ± 0.21	415.3 ± 18.9
SPIONs + BOXI-PEI	1:0.5	0.140 ± 0.010	144.5 ± 7.4

3.3.2. Zeta Potential

As expected, SPIONs coated with $PURO_{G4}$, or BOXI-PEI were approximately neutral. This can be explained by the chemical structure of $PURO_{G4}$ (cf. Figure 1.4), which shows zwitterionic functional groups. Since with the oxidation of b-PEI, it is expected to have the same terminal groups, it is also expected to have an overall neutral charge. Uncoated SPIONs are strongly anionic.

Since the compounds used for the coating are supposed to be biocompatible, and the resulting zeta potential is not strongly cationic, it's expected for these solutions to have low toxicity as they, probably, won't disrupt the cellular membrane, which is usually negatively charged [33].

Table 3.7 – Zeta potential measurements for uncoated SPIONs and for SPIONs coated with $PURO_{G4}$ and BOXI-PEI. All the solutions had a pH of 5.5.

	Zeta Potential (mV)
Uncoated SPIONs	-33.43
SPIONs + $PURO_{G4}$	1.730
SPIONs + BOXI-PEI	-5.630

3.3.3. TEM Images

The two different systems were analyzed by TEM, one where the SPIONs were functionalized with $PURO_{G4}$ and one other functionalized with BOXI-PEI. Furthermore, a third sample was analyzed, a solution with SPIONs coated with BOXI-PEI in a concentration higher than 5 mg/mL, in order to understand if the solution has a different appearance in comparison with the first two, which might be causing the difference behavior observed in this type of solution. Pristine iron oxide nanoparticles or non-coated iron oxide nanoparticles synthesized by co-precipitation were already analyzed in a published study, where it was found that the mean particle size was 9-10 nm with a narrow size distribution of 6-16 nm (Appendix A.3) [26].

Considering Figure 3.2, 3.3 and 3.4, it is possible to see that the three samples appear to have a high aggregation, this however can't lead to conclusions in terms of the efficiency of the coating used as this aggregation might be due to the accumulation of the nanoparticles in the metal grid used in the analysis. In terms of size distribution, it was possible to obtain a narrow size distribution for the three different samples. The SPIONs coated with $PURO_{G4}$ has a mean diameter of 11.18 ± 2.44 nm and the SPIONs coated with BOXI-PEI has a mean diameter of 11.37 ± 2.74 nm. Additional TEM images of the 3 different samples are available in Appendix A.4.

Between the three images and size distribution graphs, it is not possible to pinpoint the reason for the different behavior in samples of SPIONs coated with BOXI-PEI in higher concentrations than 5 mg/mL, represented in Figure 3.4. It's not possible to conclude about the high aggregation displayed in the three samples, as the nanoparticles may agglomerate in the metal grid. Further TEM analysis should be done, using more diluted samples.

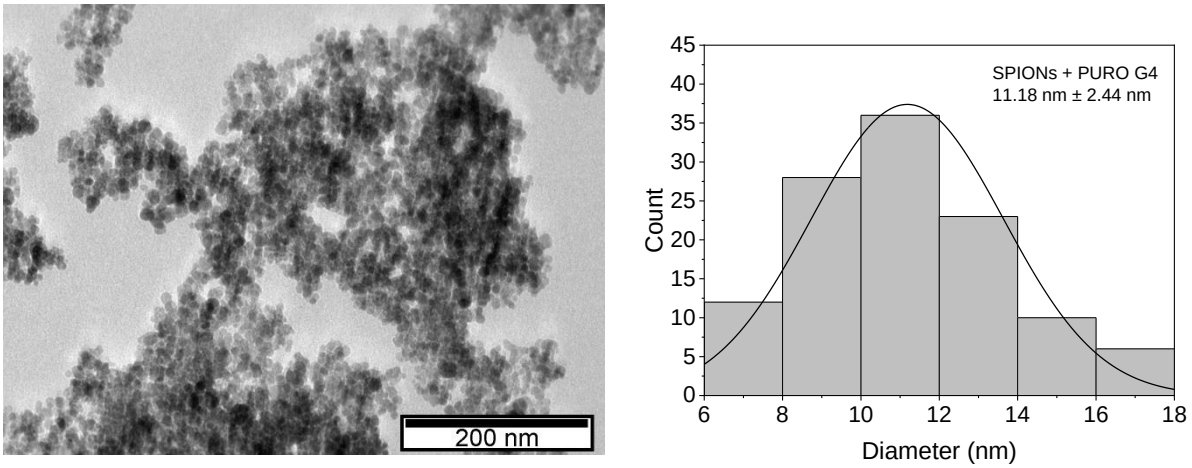

Figure 3.2 – TEM image (left) and respective size distribution graph (right) of SPIONs coated with $PURO_{G4}$ with the concentration of 0.5 mg/mL, calculated using *ImageJ™* software.

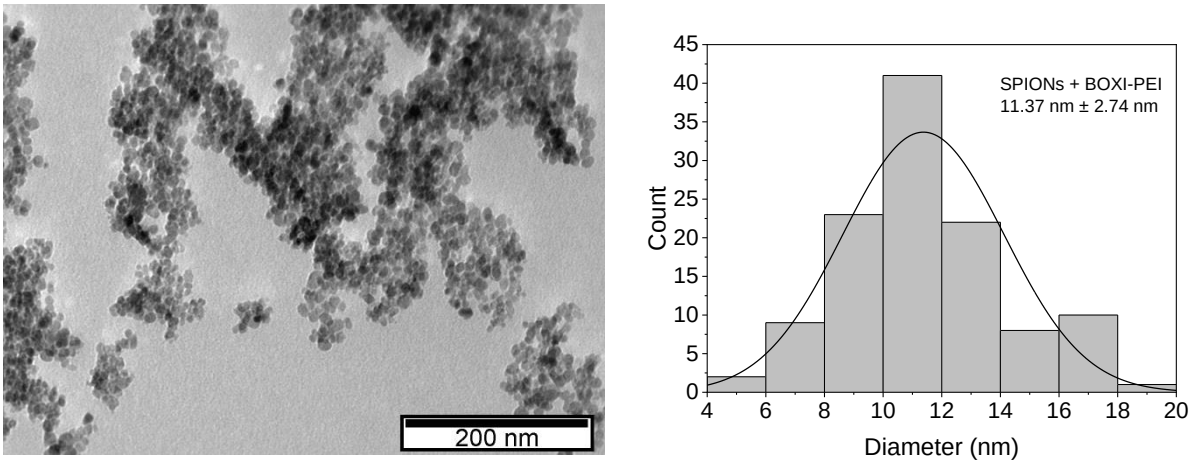

Figure 3.3 – TEM image (left) and respective size distribution graph (right) of SPIONs coated with BOXI-PEI with the concentration of 0.5 mg/mL, calculated using *ImageJ*[TM] software.

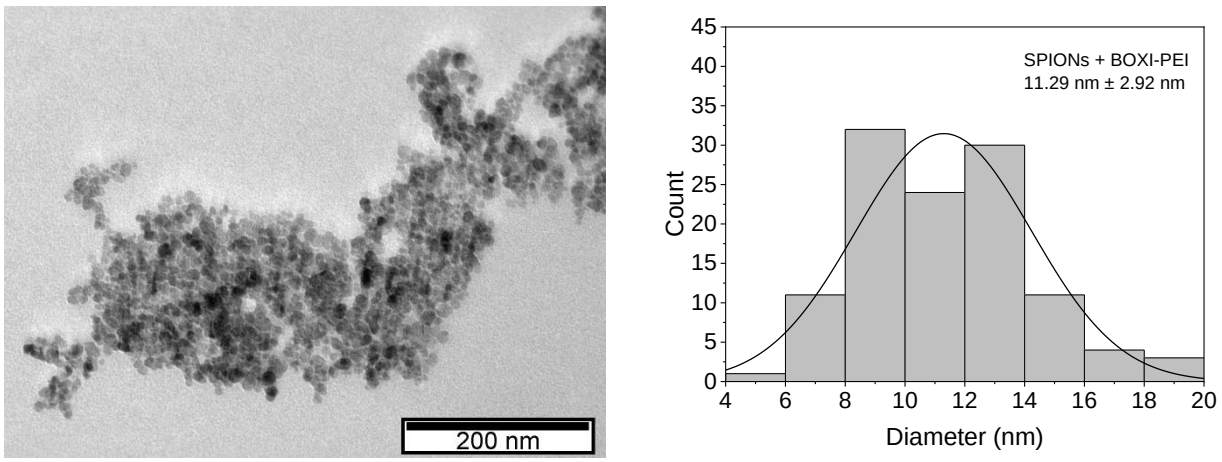

Figure 3.4 – TEM image (left) and respective size distribution graph (right) of SPIONs coated with BOXI-PEI with the concentration of 6 mg/mL, calculated using ImageJ[TM] software.

3.3.4. Magnetic Hyperthermia

To understand the influence of both coatings in the heating generation ability of the iron oxide nanoparticles, magnetic hyperthermia measurements were performed. Specific absorption rate (SAR) is defined by the amount of energy converted into heat in the unit of time and mass, quantifying the heating capacity of a magnetic material [34]. The calculation of SAR was made through the equation used by Soares *et al.* [35], presented below,

$$SAR(W/\mathrm{g}) = \frac{C_{NP} m_{Fe} + C_l m_l}{m_{Fe}} \left(\frac{dT}{dt}\right)_{max} \quad (1)$$

where $(dT/dt)_{max}$ is the maximum slope of the temperature curve, C_{NP} is the specific heat of the nanoparticles, C_l is the specific heat of the liquid, which in this case is water, m_l is the fluid mass and m_{Fe} is the iron mass. The SAR will depend the on characteristics of the NPs, like size, polydispersity, and saturation magnetization, and also on the frequency and intensity of the alternating magnetic field [36].

In Figure 3.5, the heating capacity of the uncoated SPIONs and SPIONs coated with both studied coatings were compared, additionally, using the same method, the SAR was calculated, this time for

samples with a concentration of SPIONs of 9.5 mg/mL, the three samples were compared in a graph presented in Appendix A.5.

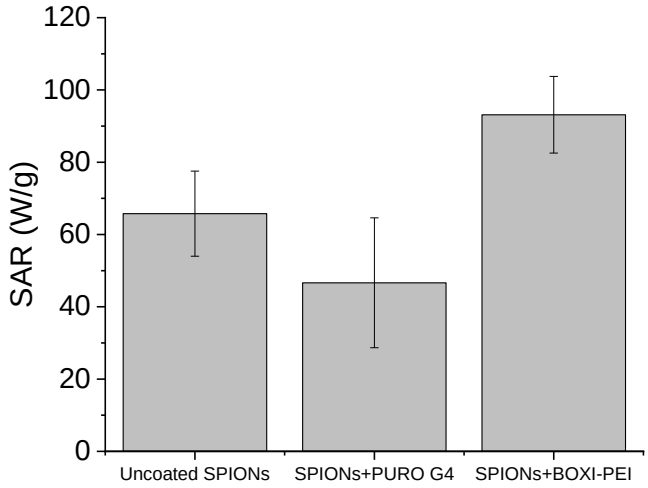

Figure 3.5 – Comparison of SAR values of uncoated SPIONs, SPIONs coated with $PURO_{G4}$ and SPIONs coated with BOXI-PEI with the concentration of 1 mg/mL. Mean ± Standard Deviation for every determination is shown.

When comparing the SAR value of the uncoated SPIONs, the sample of SPIONs coated with $PURO_{G4}$ appears to have a lower SAR value, although when taking into account the standard deviations of both samples the difference in values appears to be less relevant. In the case of the SPIONs coated with BOXI-PEI, in comparison with the uncoated SPIONs, there is a significant increase in the SAR, which would make this device more efficient in terms of heating capacity. In earlier studies, Gonçalves *et al.* concluded that the bare iron oxide nanoparticles have a higher SAR when compared with the coated NPs, this can be due to the layer formed by the stabilizing agents around the nanoparticles which restricts their Brownian movements when subjected to the alternating magnetic field, restricting their ability to generate heat [37]. In the case of the SPIONs coated with BOXI-PEI, although the branched polymer has a considerably higher molecular weight when compared with the dendrimer, however, when we take into account the DLS results represented in Table 3.6, the BOXI-PEI coating seem to obtain lower polydispersity indexes and hydrodynamic diameter which seem to lead to lower Brownian movements and with that, a higher SAR value.

Like it was mentioned earlier, different coatings can be used to stabilize the iron oxide nanoparticles, when using the same intensity alternating magnetic field and approximately the same frequency it is possible to compare the coatings used in this work, $PURO_{G4}$ and BOXI-PEI, with other more established coatings such as dimercaptosuccinic acid (DMSA), oleic acid and chitosan. In Gonçalves *et al.* study, the SAR values of uncoated NPs, nanoparticles coated with oleic acid, and nanoparticles coated with DMSA are compared, while NPs coated with oleic acid show a lower SAR value of around 75 W/g in comparison with the SAR value of 95 W/g of the uncoated NPs. NPs with DMSA have a higher SAR value of 150 W/g. In comparison with our study, NPs coated with BOXI-PEI can be considered a better coating than oleic acid but still, DMSA seems to be more efficient in terms of heating capacity [37].

Additionally, in Table 3.8 and Figure 3.6, it is possible to see the temperature variation achieved by the magnetic hyperthermia study.

Table 3.8 – Temperature variation of uncoated SPIONs, SPIONs coated with $PURO_{G4}$ and SPIONs coated with BOXI-PEI with the concentration of 1 mg/mL and 10 mg/mL. Mean±Standard Deviation for every determination is shown, except for the sample of SPIONs + BOXI-PEI with the concentration of 10 mg/mL, as only one repetition was made, the particles after the 10 minutes had the temperature of 100ºC which is unsafe for the equipment.

	1 mg/mL	9.5 mg/mL
SPIONs	5.00 ± 0.64	64.5 ± 1.2
SPIONs + $PURO_{G4}$	2.67 ± 0.050	60.2 ± 0.080
SPIONs + BOXI-PEI	6.20 ± 0.29	70.5

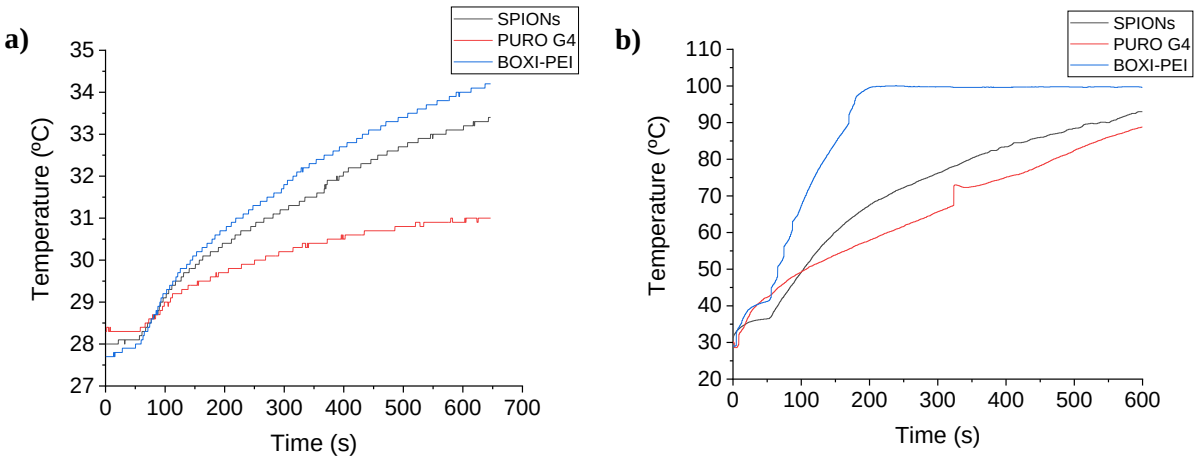

Figure 3.6 - Temperature variation of uncoated SPIONs, SPIONs coated with $PURO_{G4}$ and SPIONs coated with BOXI-PEI with concentration of a) 1 mg/mL; b) 9.5 mg/mL.

Since one of the variables that most affect the SAR value is colloidal stability, the size of the nanoparticles was measured for one month period by DLS, to understand the rate of agglomeration of the coated particles. The solutions had a concentration of 1 mg/mL, and they were stored at 9 ºC. On the measurement's days, the solution was diluted, sonicated, and analyzed through DLS.

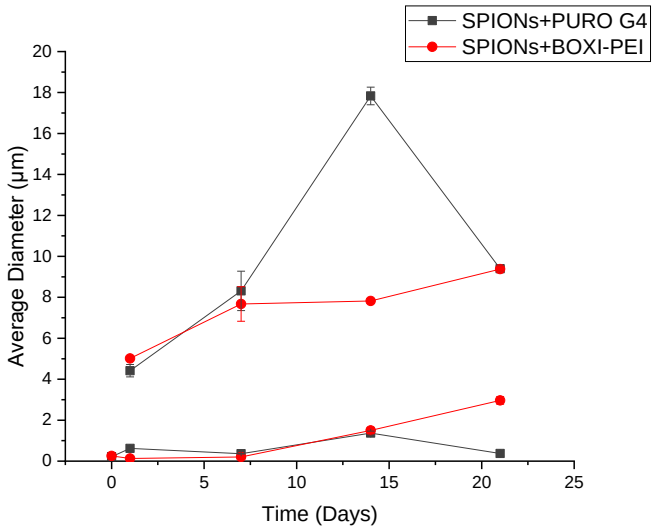

Figure 3.7 - Dynamic light scattering characterization of SPIONs coated with PURO and of SPIONs coated with BOXI-PEI through 21 days. Mean ± Standard Deviation for every determination is shown.

As we can see in Figure 3.7, both systems on day 0, that is, on the day for the synthesis, they have a similar diameter of about 200 nm. On day 1 and onward, it is possible to observe that both solutions have two populations of particles in the dispersion, one bigger population of particles which have a closer diameter to the one of day 0 and one smaller population of particles closer to the range of 4000 nm. After day 0, the percentage of particles per population appears be overall constant, while the particles diameters in both populations seem to, in general, increase over the days.

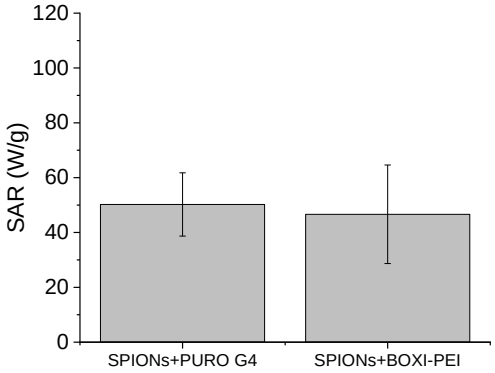

Figure 3.8 - Comparison of SAR values of SPIONs coated with $PURO_{G4}$ and SPIONs coated with BOXI-PEI with the concentration of 1 mg/mL after 21 days. Mean ± Standard Deviation for every determination is shown.

As expected, due to the agglomeration of the particles and higher polydispersity index with time, there is a considerable decrease of the SAR values and consequently, of the heating capacity of the coated nanoparticles (cf. Figures 3.5 and 3.8). And even thought, due to the standard deviation obtained in this study it is not possible conclude definitely witch system has a higher SAR value after the 21 days, it is possible to see that the SAR value of the SPIONs functionalized with BOXI- PEI suffer a more dramatic decrease when compared with the system with $PURO_{G4}$. An explanation for this agglomeration, since there is the existence of two population of particles with a different range of diameters, might be the existence of particles without coating or that aren't completely surrounded by dendrimers or branched polymers leading them to aggregate due to their positive charge.

3.3.5. NMR Relaxation

To understand if this system, in addition to being able to be used for magnetic hyperthermia treatments, can also be used as a contrast agent for MRI imaging, in a preliminary study, we evaluated the relaxation times T1 and T2 by NMR.

Considering the solution with SPIONs coated with $PURO_{G4}$, when this was transferred to a NMR tube, a rapid aggregation of the complexes and sedimentation was observed in the first minutes. As seen in Figure 3.9, only a few minutes are enough to see considerable sedimentation.

a) b) c)

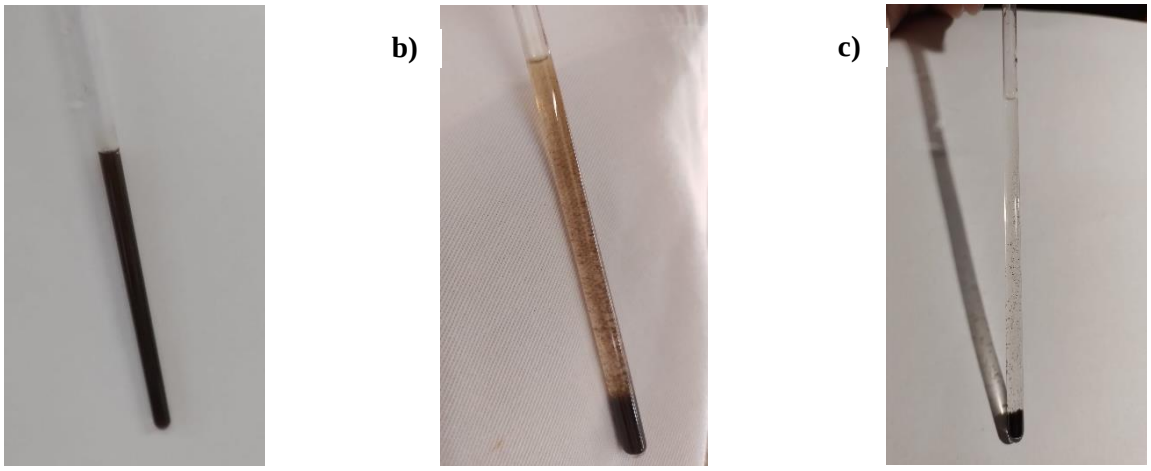

Figure 3.9 – Solution of SPIONs functionalized with $PURO_{G4}$, a) at the time of transfer to the NMR tube, b) after 10 minutes, c) after 3 hours.

With that in mind, it is not possible to have certainty in the conclusions obtained in the analysis made using NMR. In Table 3.9, it is possible to observe two types of T1 relaxation times, one fast and one slow, which indicates a biexponential behavior. Considering the observed sedimentation, it seems that the particles have a fast T1 relaxation time and as the particles aggregate and descend to the bottom of the tube, the population decreases. At the same time, as in the window analysis will become mainly water, we see the population of the slow T1 relaxation time increase. And although it does make sense, and having a reduced T1 relaxation time is a good indicator of the possibility of using this system for contrast agents, we don't have certainty in this conclusion.

Table 3.9 – Nuclear magnetic resonance characterization of SPIONs functionalization with $PURO_{G4}$. T1 is the longitudinal relaxation time.

	$T1_{fast}$ (s)	$Population_{fast}$	$T1_{slow}$ (s)	$Population_{slow}$
Replica 1	0.2492	96 %	1.843	4 %
Replica 2	0.2795	63 %	1.842	37 %
Replica 3	0.2910	25 %	1.910	75 %

In the future, one possible application for our system will be its integration on a gel type material, for the use as a filler for bone voids that result from surgery. The use of a system with theranostic and bone regeneration proprieties would allow the monitorization and therapy for remaining cancer cells, triggering an accelerated osteogenic differentiation. In this case, as the system would be applied in a gel matrix, the low stability and high sedimentation rates observed would be less important. Thus, it would be interesting to further study the properties of this system in a medium closer to the one which will be used in the final application as the medium will influence the heating capacity and as it would be possible to get a more concrete conclusion in relation to the possibility of the use of this system as contrast agents in MRI.

3.3.6. Cytotoxicity Assay

Before evaluating the cytotoxicity of the system, it is important to know the cytotoxicity of each component separately. In the work of Pires et al., a big range of concentrations of PURO, between 0 to 10 mg/mL were tested [16]. It was concluded that PURO, and specifically $PURO_{G4}$ does not cause glutathione depletion and hence, no oxidative damage was found even for high concentrations.

For the cytotoxicity of uncoated SPIONs and BOXI-PEI, a resazurin assay was performed to evaluate the relative cell viability, presented in Figure 3.10, respectively. As it was expected, BOXI-PEI can be considered not cytotoxic since there is only a lowering in the relative cell viability in the last studied concentration, and even that last one concentration could be used since the viability is still higher than 85%. As for the relative cell viability of uncoated SPIONs, and in par with the published literature, these can be considered somewhat cytotoxicity especially in higher concentrations [35]. However, when working with coated nanoparticles, it is the surface properties of the device that need to be particularly investigated in more detail since these properties seem to be the determining factor for cell uptake and cytotoxicity.

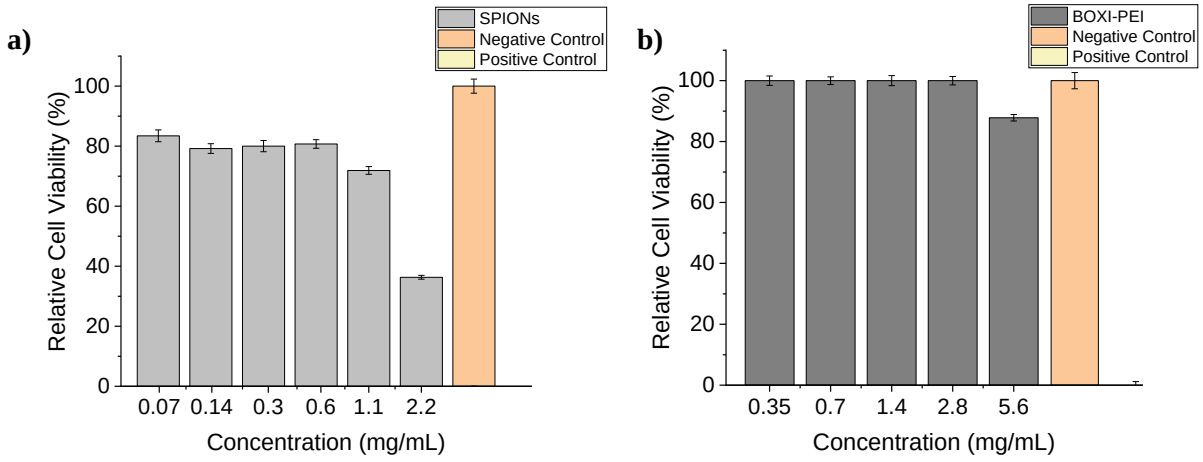

Figure 3.10 - Relative cell viability of a) uncoated SPIONs; b) BOXI-PEI.

As a first approach, in order to understand the relative cell viability of the nanoparticles coated with $PURO_{G4}$ and of the nanoparticles coated with BOXI-PEI, two resazurin assay were performed, in which the obtained results are presented in Figure 3.11. It is possible to understand that the solution of SPIONS with a $PURO_{G4}$ coating is less cytotoxic in comparison with the BOXI-PEI coating. Furthermore, it was not possible to get higher than about 50% relative cell viability in the case of the samples of SPIONs with BOXI-PEI. To understand if this was indeed the effect that the device had on the cells or if, as it happened in a previous study where the nanoparticles were coated with (3-aminopropyl) triethoxysilane (APTES), there was an aggregation of NPs in the cells membrane which made difficult the entrance and metabolization of the resazurin in the cells, a final resazurin assay was done, this time just with SPIONs coated with BOXI-PEI but in minimal concentrations, as presented in Figure 3.11. [38]

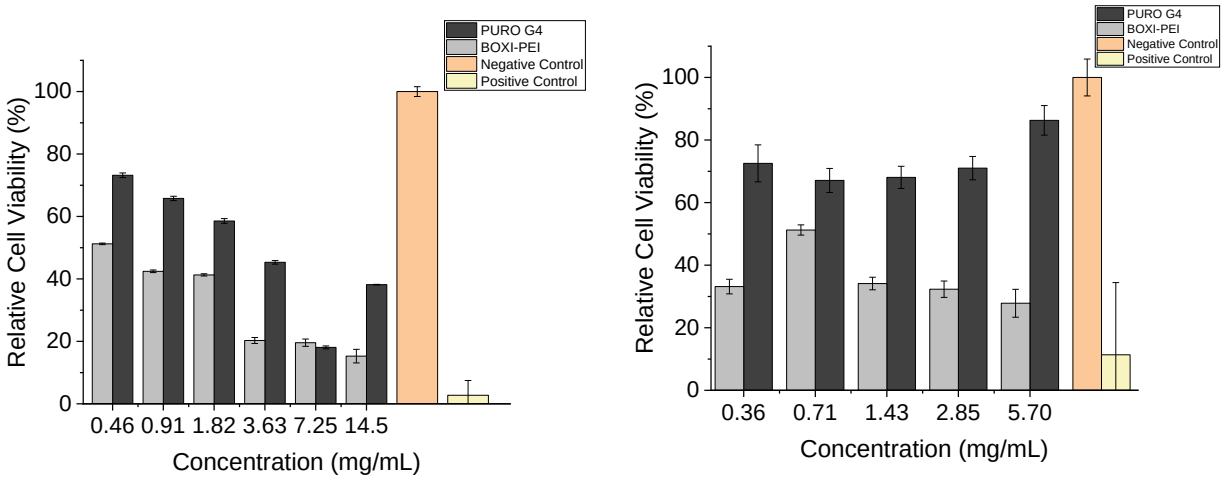

Figure 3.11 - Relative cell viability of SPIONs coated with $PURO_{G4}$ and SPIONs coated with BOXI-PEI obtained using the resazurin assay.

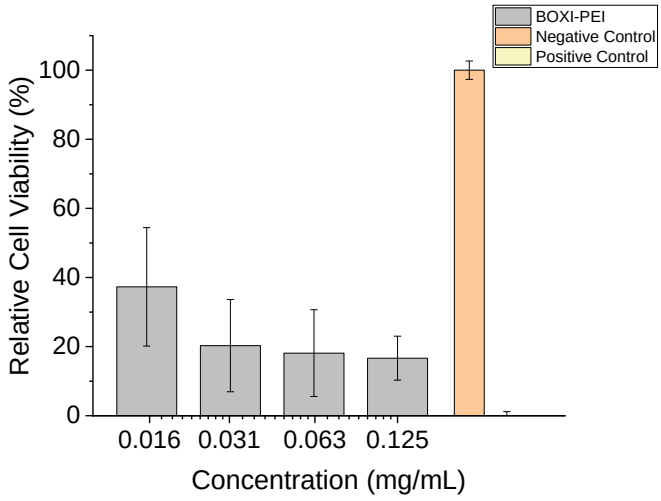

Figure 3.12 - Relative ell viability of SPIONs coated with BOXI-PEI obtained using the resazurin assay.

A live and dead assay was also performed, and the results are shown in Figure 3.13. As it is possible to see, the limitation in getting higher relative cell viability for the solutions of SPIONs with a BOXI-PEI coating was overcome, being able to get relative cell viability of about 90% on a concentration of 0.5 mg/mL, which is considered non-cytotoxic. Furthermore, it is possible to observe a similar effect when comparing Figure3.13 to Figure 3.11b, where, contrary to what would be expected, an increase of concentration of 0.36 to 0.71 mg/mL, leads to an increase in the relative cell viability, lowering again when the concentration increases from 0.71 to 1.43 mg/mL. In Figure 3.13, we see an increase when the concentration goes from 0.2 to 0.5 and then a decrease when the concentration goes from 0.5 to 1 mg/mL. It would be expected that the lower concentration would have the higher relative cell viability and that this value would increase as the concentrations also increases. It is though that in the lowest concentrations of the system of SPIONs coated with BOXI-PEI tested could be having a harder time entering the cells, and with slight increase in the concentration the system seem to enter the cells, the hydroxylamine-terminated surface of the polymer may lead to catalase enzymes signaling, which promotes an increase in production of nitric oxide. It has been proven that, in small quantities, NO exhibits a protective effect as a chain-breaking antioxidant [39]. To better understand the behavior and influence of the SPIONs functionalized with BOXI-PEI a further cell uptake study should be done, both of the system and of the polymer.

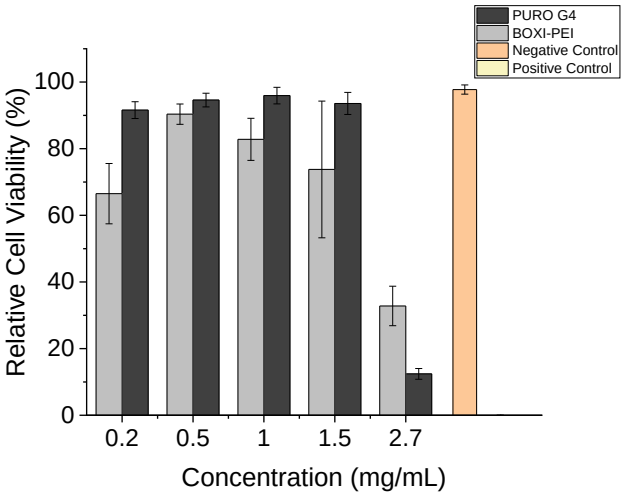

Figure 3.13 - Relative cell viability of SPIONs coated with $PURO_{G4}$ or with BOXI-PEI obtained in live and dead assay.

4. CONCLUSION

The objective of this work was to develop a hybrid therapeutic formulation that combines superparamagnetic iron oxide nanoparticles with PURO dendrimer or oxidized poly(ethylene imine) polymer. Since both polymers have the same terminal functional groups (hydroxylamine), which trigger osteodifferentiation of hMSCs by nitric oxide (NO) *in situ* release by the action of catalase, the goal was to obtain a system that could combine the theranostic properties of the SPIONs with bone regeneration.

To obtain the target functionalized system, two main approaches were taken, the first was to initially functionalize the SPIONs with citric acid, which has been proven to lead to small monodisperse particles, and then further functionalize the system with the dendrimer or the branched polymer. However, when this last element was added to the solution, the CA coating was destabilized, making it difficult to obtain the needed properties. The second approach taken was a functionalization only with PURO or BOXI-PEI. During this approach, it was possible to obtain an optimized protocol, where the solution of SPIONs with polymers are submitted to an ultrasound bath for 1 hour and 30 minutes. It was also possible to optimize the ratios in order to obtain nanoparticles with low polydispersity index and a small diameter. The preferred ratios were 1:1 of SPIONs:$PURO_{G4}$ and 1:0.5 of SPIONs:BOXI-PEI.

Throughout the process of reaching an optimized method and ratios, several analyses by DLS were made, where the optimized results were of monodispersed solutions with a system diameter of 415.3±18.9 for SPIONs coated with $PURO_{G4}$ and 144.5±7.5 for SPIONs coated with BOXI-PEI. Furthermore, through a zeta potential analysis, it was possible to conclude that both systems have overall neutral charge. To have a better understanding of the size and aggregation of the nanoparticles, a TEM analysis was conducted where it was possible to observe a particle diameter of around 10 nm in both systems. Yet, a further TEM analysis should be made, with more diluted samples, to understand whether the aggregation of the particles observed is due to aggregation to the metal grid used in the analysis or an aggregation due to instability of the system.

To access the theranostic properties of the developed platforms, it was first done a magnetic hyperthermia analysis, where it was possible to understand that SPIONs+$PURO_{G4}$ exhibit a slight lower SAR value and that SPIONs+BOXI-PEI a slightly higher SAR value when compared with the SAR value of uncoated SPIONs. When compared with the SAR value of other SPIONs coatings present in the literature, the values of SAR of the SPIONs+BOXI-PEI being higher than oleic acid coating, but lower when compared with DMSA . However, it is important to note, that a colloidal stability study was done, and when considering the agglomeration after one month, the SAR values of SPIONs+BOXI-PEI had a significant decrease while the SAR value of SPIONS+$PURO_{G4}$ seem to be less affected. The NMR

relaxation was analyzed where it was not possible to obtain a definitive conclusion due to the agglomeration of particles and consequent sedimentation, however it gave us positive enough hints to understand that a following study should be done in a medium more close to the one that is going to be used in the final application of this system.

Finally, since we target a biomedical application, it was important to evaluate the cytotoxicity of the platform. First, following the study done by Pires *et al.* [16] where it was found that the $PURO_{G4}$ was not toxic, a resazurin assay was done with uncoated SPIONs and after with BOXI-PEI, where both individually were found to be non-cytotoxic. For the system of SPIONs+BOXI-PEI, it was not possible to get many conclusions through a resazurin assay as it is possible that an aggregation of nanoparticles in the cell membrane made difficult the entrance and further metabolization of the resazurin in the cell. Thus, a live dead assay was performed where it was concluded that the system SPIONs+$PURO_{G4}$ is non cytotoxic up to 1.5mg/mL while SPIONs+BOXI-PEI is non cytotoxic in the range of 0.5-1 mg/mL. A further live dead assay could be done to get a concrete conclusion on the cytotoxicity of the system SPIONs+BOXI-PEI with a concentration of 1.5 mg/mL.

Future research should focus on the bone regeneration properties of the systems with alizarin red staining and alkaline phosphatase activity assay to access the osteogenic differentiation in hMSCs cells.

BIBLIOGRAPHY

[1] "Cancer." https://www.who.int/news-room/fact-sheets/detail/cancer (accessed Oct. 03, 2022).

[2] M. G. Cecchini, A. Wetterwald, G. van der Pluijm, and G. N. Thalmann, "Molecular and biological mechanisms of bone metastasis," *EAU Updat. Ser.*, vol. 3, no. 4, pp. 214–226, 2005, doi: 10.1016/j.euus.2005.09.006.

[3] F. Macedo *et al.*, "Bone Metastases: An Overview," *Oncol. Rev.*, vol. 11, no. 1, Mar. 2017, doi: 10.4081/ONCOL.2017.321.

[4] R. L. Jilka, "Biology of the basic multicellular unit and the pathophysiology of osteoporosis," *Med. Pediatr. Oncol.*, vol. 41, no. 3, pp. 182–185, Sep. 2003, doi: 10.1002/MPO.10334.

[5] "Definition of metastasis - NCI Dictionary of Cancer Terms - NCI." https://www.cancer.gov/publications/dictionaries/cancer-terms/def/metastasis (accessed Oct. 03, 2022).

[6] G. R. Mundy, "Metastasis to bone: Causes, consequences and therapeutic opportunities," *Nat. Rev. Cancer*, vol. 2, no. 8, pp. 584–593, 2002, doi: 10.1038/nrc867.

[7] V. Vassiliou and D. Kardamakis, "Combined Radiotherapy and Bisphosphonates: State of Art," pp. 233–250, 2009, doi: 10.1007/978-1-4020-9819-2_11.

[8] P. I. P. Soares, J. Romão, R. Matos, J. C. Silva, and J. P. Borges, "Design and engineering of magneto-responsive devices for cancer theranostics: Nano to macro perspective," *Prog. Mater. Sci.*, vol. 116, no. October 2020, p. 100742, 2021, doi: 10.1016/j.pmatsci.2020.100742.

[9] A. Akbarzadeh, M. Samiei, and S. Davaran, "Magnetic nanoparticles: Preparation, physical properties, and applications in biomedicine," *Nanoscale Res. Lett.*, vol. 7, no. 1, pp. 1–13, Feb. 2012, doi: 10.1186/1556-276X-7-144/FIGURES/3.

[10] E. Spain and A. Venkatanarayanan, *Review of Physical Principles of Sensing and Types of Sensing Materials*, vol. 13. Elsevier, 2014.

[11] X. Chen and S. T. C. Wong, "Cancer Theranostics: An Introduction," *Cancer Theranostics*, pp. 3–8, 2014, doi: 10.1016/B978-0-12-407722-5.00001-3.

[12] A. C. Anselmo and S. Mitragotri, "Nanoparticles in the clinic: An update," *Bioeng. Transl. Med.*, vol. 4, no. 3, Sep. 2019, doi: 10.1002/BTM2.10143.

[13] J. M. Oliveira, A. J. Salgado, N. Sousa, J. F. Mano, and R. L. Reis, "Dendrimers and derivatives as a potential therapeutic tool in regenerative medicine strategies - A review," *Prog. Polym. Sci.*, vol. 35, no. 9, pp. 1163–1194, 2010, doi: 10.1016/j.progpolymsci.2010.04.006.

[14] D. T. Mlynarczyk, T. Kocki, T. Goslinski, D. T. Mlynarczyk, T. Kocki, and T. Goslinski, "Dendrimer Structure Diversity and Tailorability as a Way to Fight Infectious Diseases," *Nanostructured Mater. - Fabr. to Appl.*, Jul. 2017, doi: 10.5772/67660.

[15] E. Abbasi *et al.*, "Dendrimers: Synthesis, applications, and properties," *Nanoscale Res. Lett.*, vol. 9, no. 1, pp. 1–10, 2014, doi: 10.1186/1556-276X-9-247.

[16] R. F. Pires, J. Conde, and V. D. B. Bonifácio, "Osteogenic Differentiation of Human Mesenchymal Stem Cells by the Single Action of Luminescent Polyurea Oxide Biodendrimers," *ACS Appl. Bio Mater.*, vol. 3, no. 12, pp. 9101–9108, 2020, doi: 10.1021/acsabm.0c01315.

[17] R. B. Restani *et al.*, “Polyurea dendrimer for efficient cytosolic siRNA delivery,” *RSC Adv.*, vol. 4, no. 97, pp. 54872–54878, 2014, doi: 10.1039/c4ra09603g.

[18] L. M. Bronstein and Z. B. Shifrina, “Dendrimers as encapsulating, stabilizing, or directing agents for inorganic nanoparticles,” *Chem. Rev.*, vol. 111, no. 9, pp. 5301–5344, 2011, doi: 10.1021/cr2000724.

[19] S. Chandra, S. Nigam, and D. Bahadur, “Combining unique properties of dendrimers and magnetic nanoparticles towards cancer theranostics,” *J. Biomed. Nanotechnol.*, vol. 10, no. 1, pp. 32–49, 2014, doi: 10.1166/jbn.2014.1698.

[20] Z. Bober, D. Bartusik-Aebisher, and D. Aebisher, “Application of Dendrimers in Anticancer Diagnostics and Therapy,” *Molecules*, vol. 27, no. 10, pp. 1–19, 2022, doi: 10.3390/molecules27103237.

[21] V. Haribabu, A. S. Farook, N. Goswami, R. Murugesan, and A. Girigoswami, “Optimized Mn-doped iron oxide nanoparticles entrapped in dendrimer for dual contrasting role in MRI,” *J. Biomed. Mater. Res. - Part B Appl. Biomater.*, vol. 104, no. 4, pp. 817–824, 2016, doi: 10.1002/jbm.b.33550.

[22] Y. Chang *et al.*, “Novel water-soluble and pH-responsive anticancer drug nanocarriers: Doxorubicin-PAMAM dendrimer conjugates attached to superparamagnetic iron oxide nanoparticles (IONPs),” *J. Colloid Interface Sci.*, vol. 363, no. 1, pp. 403–409, 2011, doi: 10.1016/j.jcis.2011.06.086.

[23] K. Wu, B. Yu, D. Li, Y. Tian, Y. Liu, and J. Jiang, “Recent Advances in Nanoplatforms for the Treatment of Osteosarcoma,” *Front. Oncol.*, vol. 12, no. February, pp. 1–18, 2022, doi: 10.3389/fonc.2022.805978.

[24] G. Niu *et al.*, “Melatonin and doxorubicin co-delivered via a functionalized graphene-dendrimeric system enhances apoptosis of osteosarcoma cells,” *Mater. Sci. Eng. C*, vol. 119, no. August 2019, p. 111554, 2021, doi: 10.1016/j.msec.2020.111554.

[25] C. Englert *et al.*, “Enhancing the Biocompatibility and Biodegradability of Linear Poly(ethylene imine) through Controlled Oxidation,” *Macromolecules*, vol. 48, no. 20, pp. 7420–7427, Oct. 2015, doi: 10.1021/ACS.MACROMOL.5B01940/SUPPL_FILE/MA5B01940_SI_001.PDF.

[26] P. I. P. Soares *et al.*, “Effects of surfactants on the magnetic properties of iron oxide colloids,” *J. Colloid Interface Sci.*, vol. 419, pp. 46–51, Apr. 2014, doi: 10.1016/J.JCIS.2013.12.045.

[27] M. A. Dheyab, A. A. Aziz, M. S. Jameel, O. A. Noqta, P. M. Khaniabadi, and B. Mehrdel, “Simple rapid stabilization method through citric acid modification for magnetite nanoparticles,” *Sci. Reports 2020 101*, vol. 10, no. 1, pp. 1–8, Jul. 2020, doi: 10.1038/s41598-020-67869-8.

[28] T. Vieira, J. Carvalho Silva, A. M. Botelho do Rego, J. P. Borges, and C. Henriques, “Electrospun biodegradable chitosan based-poly(urethane urea) scaffolds for soft tissue engineering,” *Mater. Sci. Eng. C*, vol. 103, no. May, p. 109819, 2019, doi: 10.1016/j.msec.2019.109819.

[29] G. J. Kontoghiorghes, “2-Hydroxypyridine-N-oxides: effective new chelators in iron mobilisation,” *Biochim. Biophys. Acta*, vol. 924, no. 1, pp. 13–18, Apr. 1987, doi: 10.1016/0304-4165(87)90065-1.

[30] T. Granath, K. Mandel, P. Löbmann, T. Granath, K. Mandel, and P. Löbmann, “The Significant Influence of the pH Value on Citrate Coordination upon Modification of Superparamagnetic Iron Oxide Nanoparticles,” *Part. Part. Syst. Charact.*, vol. 39, no. 3, p. 2100279, Mar. 2022, doi: 10.1002/PPSC.202100279.

[31] “The principles of dynamic light scattering :: Anton Paar Wiki.” https://wiki.anton-paar.com/en/the-principles-of-dynamic-light-scattering/ (accessed Jan. 20, 2023).

[32] O. Oehlsen, S. I. Cervantes-Ramírez, P. Cervantes-Avilés, and I. A. Medina-Velo, "Approaches on Ferrofluid Synthesis and Applications: Current Status and Future Perspectives," *ACS Omega*, vol. 7, no. 4, pp. 3134–3150, 2022, doi: 10.1021/acsomega.1c05631.

[33] J. D. Clogston and A. K. Patri, "Zeta potential measurement," *Methods Mol. Biol.*, vol. 697, pp. 63–70, 2011, doi: 10.1007/978-1-60327-198-1_6.

[34] R. R. Wildeboer, P. Southern, and Q. A. Pankhurst, "On the reliable measurement of specific absorption rates and intrinsic loss parameters in magnetic hyperthermia materials," *J. Phys. D. Appl. Phys.*, vol. 47, no. 49, p. 495003, Nov. 2014, doi: 10.1088/0022-3727/47/49/495003.

[35] P. I. P. Soares *et al.*, "Iron oxide nanoparticles stabilized with a bilayer of oleic acid for magnetic hyperthermia and MRI applications," *Appl. Surf. Sci.*, vol. 383, pp. 240–247, 2016, doi: 10.1016/j.apsusc.2016.04.181.

[36] C. Pucci, A. Degl'innocenti, M. B. Gümüş, and G. Ciofani, "Biomaterials Science REVIEW Superparamagnetic iron oxide nanoparticles for magnetic hyperthermia: recent advancements, molecular effects, and future directions in the omics era," *Cite this Biomater. Sci*, vol. 10, p. 2103, 2022, doi: 10.1039/d1bm01963e.

[37] A. Gonçalves, F. V. Almeida, J. P. Borges, and P. I. P. Soares, "Incorporation of dual-stimuli responsive microgels in nanofibrous membranes for cancer treatment by magnetic hyperthermia," *Gels*, vol. 7, no. 1, pp. 1–17, 2021, doi: 10.3390/GELS7010028.

[38] M. Vilar and S. Mateus, "Superparamagnetic Iron oxide 'nanozymes' for cancer theranostics," 2022, Accessed: Feb. 17, 2023. [Online]. Available: https://run.unl.pt/handle/10362/147263.

[39] K. D. Kröncke, K. Fehsel, and V. Kolb-Bachofen, "Nitric oxide: Cytotoxicity versus cytoprotection - How, why, when, and where?," *Nitric Oxide - Biol. Chem.*, vol. 1, no. 2, pp. 107–120, 1997, doi: 10.1006/niox.1997.0118.

APPENDIX

A.1. NMR CHARACTERIZATION

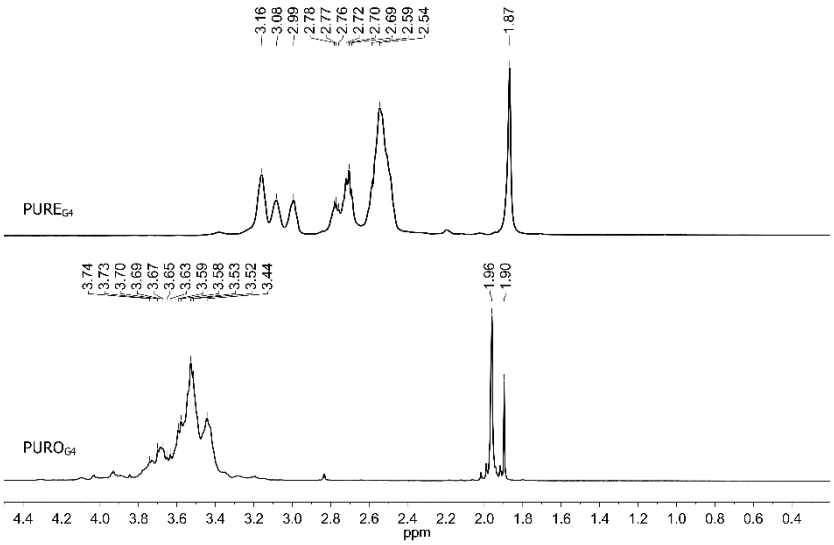

Figure A.1.1 - NMR characterization of PURE$_{G4}$ and PURO$_{G4}$ with water as the solvent.

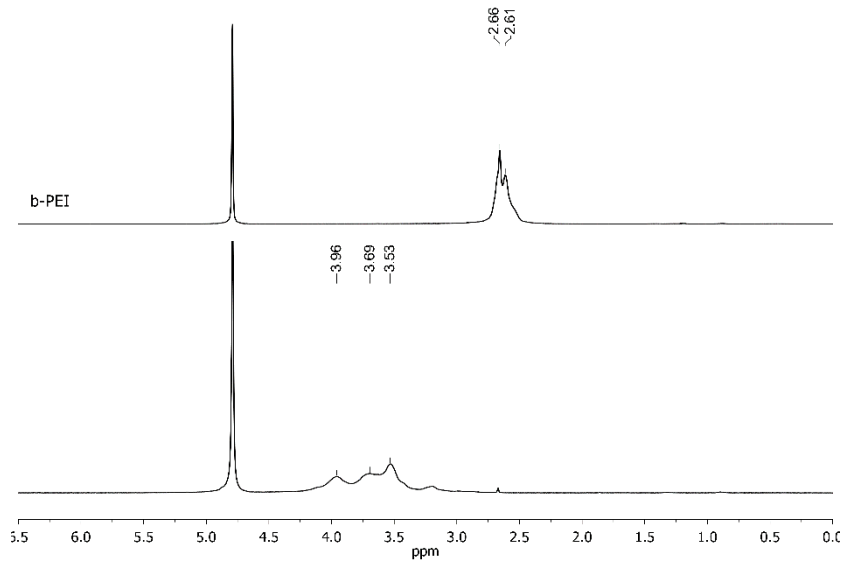

Figure A.1.2 – NMR characterization of b-PEI and BOXI-PEI with water as the solvent.

A.2. pH Measurements

Table A.2.1 – pH Measurements of different coatings, uncoated SPIONs and citric acid.

	pH
CA	2.0
Uncoated SPIONs	5.5
$PURO_{G4}$	7.0
BOXI-PEI	9.0

A.3. Pristine SPIONs TEM Images

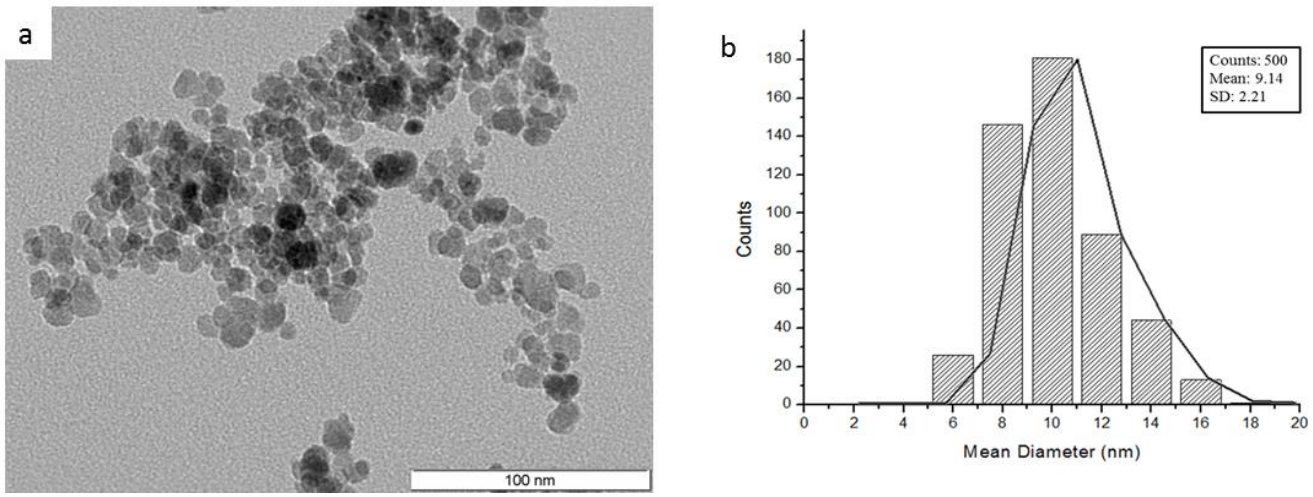

Figure A.3.1 – a) TEM image of pristine Fe_3O_4 nanoparticles; b) Size distribution calculated using *ImageJ*™ software. [26]

A.4. Additonal TEM images

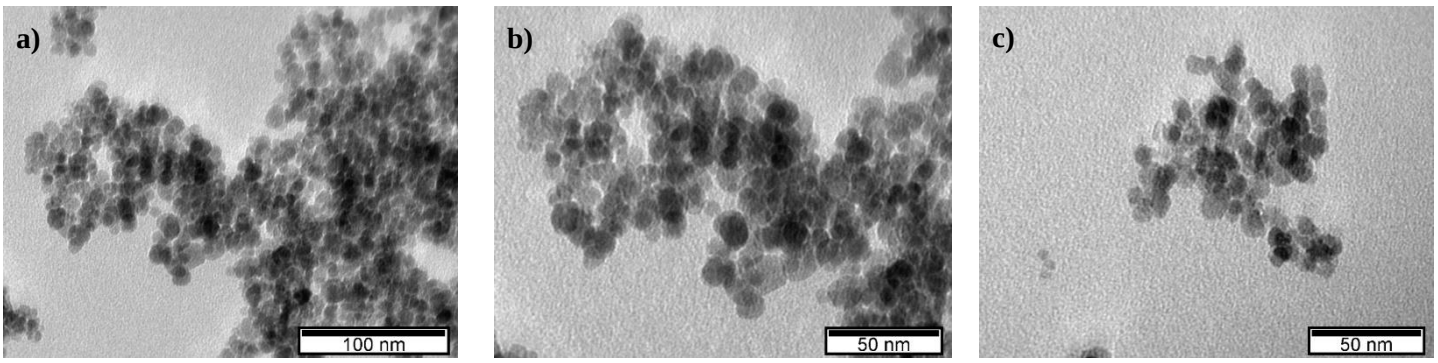

Figure A.4.1 – TEM image of SPIONs with $PURO_{G4}$ coating with a magnification of a) 80kx; b) 120kx; c)120kx.

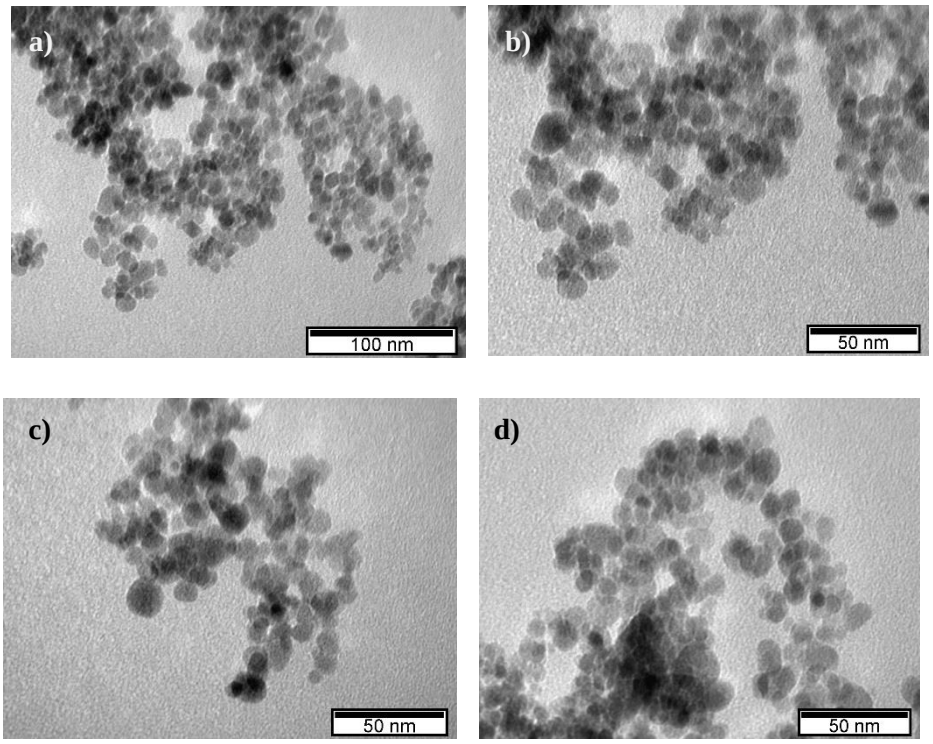

Figure A.4.2 – TEM image of SPIONs with BOXI-PEI coating with a concentration of 0.5 mg/mL with a magnification of a) 80kx; b) 120kx; c) 120kx; d) 120kx.

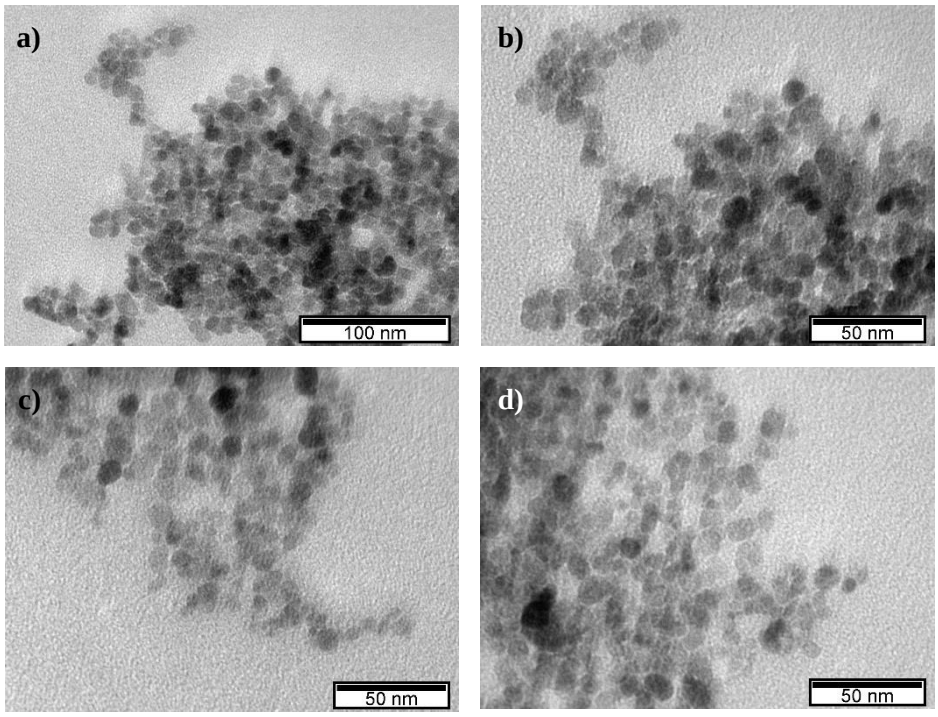

Figure A.4.3 – TEM image of SPIONs with BOXI-PEI coating with a concentration of 6 mg/mL with a magnification of a) 80kx; b) 120kx; c) 120kx; d) 120kx.

A.5. Complementary Magnetic Hyperthermia Results

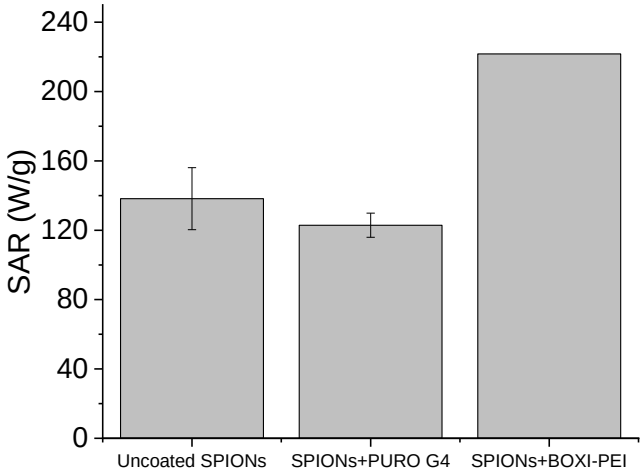

Figure A.5.1 - Comparison of SAR values of uncoated SPIONs, SPIONs coated with $PURO_{G4}$ and SPIONs coated with BOXI-PEI with concentration of 9.5 mg/mL**.** Mean±Standard Deviation for every determination is shown.